Travelling waves in discrete spatial domains

Hal, B. van

B. van Hal

Travelling waves in discrete spatial domains

Bachelor thesis

July 28, 2017

Thesis supervisor: dr. H.J. Hupkes

Leiden University
Mathematical Institute

Contents

1 Introduction

In this thesis we look at a reaction-diffusion equation in discrete space. Reaction-diffusion equations in continuous space have been used extensively to model real life situations, in areas such as biology, physics and chemistry. Typical applications feature one or more species or chemical substances that can interact with each other and spread throughout a spatial domain. As we will explain below, the interactions can be modelled by reaction terms, which do not depend on space. The spreading can be modelled by diffusion terms, which do have a spatial dependence.

1.1 Diffusion

Consider a group of rabbits on a surface $\mathcal{D} \in \mathbb{R}$, and write u for the density of the rabbits in $\mathcal{D}$. The behaviour of the rabbits is influenced by diffusion. This means that the group of rabbits will eventually spread equally in space. At a certain moment the total amount of rabbits $N_{\mathcal{D}}$ in the surface $\mathcal{D}$ is

$$N_{\mathcal{D}} = \iint_{\mathcal{D}} u dA. \tag{1}$$

We write $\overrightarrow{F}$ for the vector field corresponding to the velocity of the rabbits. Our main assumption here is that the rabbits move in the direction in which the density decreases the fastest. This can be modelled mathematically by

$$\overrightarrow{F} = -\nabla u. \tag{2}$$

We denote the total decrease of the amount of rabbits in the surface $\mathcal{D}$ with $F_{\mathcal{D}}$. This is equal to the amount of rabbits that move over the boundary $\delta\mathcal{D}$ of $\mathcal{D}$ in the outward direction, which gives

$$F_{\mathcal{D}} = \int_{\delta\mathcal{D}} \overrightarrow{F} \cdot \overrightarrow{n}\, ds. \tag{3}$$

Using the divergence theorem we can compute

$$F_{\mathcal{D}} = \iint_{D} \nabla \cdot \overrightarrow{F} dA. \tag{4}$$

Using our model (2), the decrease of the total amount of rabbits in $\mathcal{D}$ becomes

$$F_{\mathcal{D}} = -\iint_{D} \nabla \cdot \nabla u dA = \iint_{D} \Delta u dA. \tag{5}$$

The change in the amount of rabbits on the surface is equal to minus the amount of rabbits that leave the surface. This means that

$$\frac{d}{dt} N_{\mathcal{D}} = -F_{\mathcal{D}}. \tag{6}$$

Substituting the equations (1) and (5) in equation (6) gives us

$$\frac{d}{dt}\iint_{\mathcal{D}} u dA = \iint_{D} \Delta u dA.$$

Interchanging integrals and differentials, we therefore get

$$\iint_{\mathcal{D}} u_t dA = \iint_{D} \Delta u dA.$$

Since this has to hold for any surface $\mathcal{D}$, we can conclude that

$$u_t = \Delta u. \tag{7}$$

This last equation is well-known as the heat equation and plays a very important role in many processes involving diffusion.

1.2 Reaction

We discuss the reaction term with an example coming from population dynamics, based on [2].

Consider a population of cells and suppose that the gene at a specific locus in a specific chromosome pair occurs in two forms, which we denote by a and A, named "alleles". Genes occur in couples and since we have two "alleles" we have three different couples, namely aa, aA and AA, which we call genotypes. The genotype Aa is included in the genotype aA. The first and the last genotypes carry only one allele and are called homozygotes. The second genotype carries two different alleles, and is called heterozygote.

The population is distributed in a one-dimensional habitat. The linear densities of the genotypes aa, aA and AA at the point x at time t are respectively denoted by $\rho_1(x,t), \rho_2(x,t)$ and $\rho_3(x,t)$. The alleles couple at random, which means that every genotype has the same birthrate r. However, each allele has a different death rate, so the death rates of the genotypes are also different. We denote the death rate with τ_1, τ_2 and τ_3 respectively.

With the assumptions we stated before, the population densities satisfy the system of partial differential equations,

$$\begin{array}{rcl} \frac{d\rho_1}{dt} & = & \frac{d^2\rho_1}{dx^2} - \tau_1\rho_1 + \frac{r}{\rho}(\rho_1 + \frac{1}{2}\rho_2)^2 \\ \frac{d\rho_2}{dt} & = & \frac{d^2\rho_2}{dx^2} - \tau_2\rho_2 + \frac{2r}{\rho}(\rho_1 + \frac{1}{2}\rho_2)(\rho_3 + \frac{1}{2}\rho_2) \\ \frac{d\rho_3}{dt} & = & \frac{d^2\rho_3}{dx^2} - \tau_3\rho_3 + \frac{r}{\rho}(\rho_3 + \frac{1}{2}\rho_2)^2 \end{array} \tag{8}$$

in which $\rho = \rho_1 + \rho_2 + \rho_3$ denotes the total population.

In the system we see in every equation the term $\frac{d\rho_i}{dt} = \frac{d^2\rho_i}{dx^2}$, which is equal to the diffusion explained in subsection 1.1.

The term $\tau_i\rho_i$ denotes the departed genotypes in the habitat and the term $\frac{r}{\rho}(\rho_i + \frac{1}{2}\rho_2)^2$ gives the born genotypes in the habitat. Note that for the second equation we have $\frac{2r}{\rho}(\rho_1 + \frac{1}{2}\rho_2)(\rho_3 + \frac{1}{2}\rho_2)$, this is because aA can occur when allele a couples A, which gives $(\rho_1 + \frac{1}{2}\rho_2)$ and when allele A

couples a, which gives $(\rho_3 + \frac{1}{2}\rho_2)$. This means that the chance that we get the genotype aA is twice the chance that we get the genotype aa or AA.

It is easier to evaluate the behaviour of a PDE which is only dependent of one variable u,

$$u = \frac{\rho_3 + \frac{1}{2}\rho_2}{\rho_1 + \rho_2 + \rho_3}, \tag{9}$$

which denotes the percentage of allele A of all alleles.

In [2] the authors explain that the behaviour of u can be approximated by the scalar system $u_t = \Delta u + g(u)$ in which g is given by

$$g(u) = u(1-u)\left((\tau_1 - \tau_2)(1-u) - (\tau_3 - \tau_2)u\right). \tag{10}$$

This function g is called the reaction term and approximated the interaction described in (8).

To determine the behaviour of this reaction term we need the derivative of $g(u)$, which is given by

$$\frac{dg}{du} = (\tau_1 - \tau_2)(1 - 4u + 3u^2) + (\tau_3 - \tau_2)(3u^2 - 2u). \tag{11}$$

Notice that the relative values of the death rates τ_1, τ_2, τ_3 are essential for the behaviour of the reaction term. Without loss of generality, we assume that $\tau_1 > \tau_3$, which means that AA is more viable than aa.

We can distinguish three cases for the relative viability of the genotypes, where each case has a different impact on the term $((\tau_1 - \tau_2)(1-u) - (\tau_3 - \tau_2)u)$.

Case 1. If $\tau_3 \leq \tau_2 < \tau_1$, the viability of the heterozygote is in between the viability of the homozygotes, we call this heterozygote intermediate. This implies the following for equation (10),

$$\begin{array}{ll} g'(0) > 0, & \\ g(u) > 0 & \text{for } u \in (0,1). \end{array} \tag{12}$$

Case 2. If $\tau_2 < \tau_3 \leq \tau_1$, the viability of the heterozygote is better than the viability of the homozygotes, we call this heterozygote superiority. This implies that there exists an $\alpha \in (0,1)$ for which,

$$\begin{array}{lll} g'(0) > 0, & g'(1) > 0, & \\ g(u) > 0, & \text{for } u \in (0,\alpha), & \\ g(u) < 0, & \text{for } u \in (\alpha,1). & \end{array} \tag{13}$$

Case 3. If $\tau_3 \leq \tau_1 < \tau_2$, the viability of the heterozygote is worse than the viability of the homozygotes, we call this heterozygote inferiority. This implies that there exists an $\alpha \in (0,1)$ for which,

$$\begin{array}{lll} g'(0) < 0, & g'(1) < 0, & \\ g(u) < 0, & \text{for } u \in (0,\alpha), & \\ g(u) > 0, & \text{for } u \in (\alpha,1). & \end{array} \tag{14}$$

We will focus on the last case in this thesis. This case has three equilibria, namely $u = 0, u = 1$ and $u = \alpha$. We have $g'(u, \alpha) < 0$ for $u = 0$ and $u = 1$, so these are stable equilibria. For $u = \alpha$ we have $g(\alpha, \alpha) > 0$ thus the equilibrium in $u = \alpha$ is unstable. Since we have two stable equilibria, $g(u)$ is a bistable reaction term. This means that spatially constant solutions will go to 0 if $u < \alpha$ and to 1 when $u > \alpha$. In this system we can conclude that when $u < \alpha$ allele A will die out and when $u > \alpha$ allele a will die out.

1.3 The Model Equations

The Partial Differential Equation we focus on consists, like the genetic model discussed above, of a diffusionterm and a bistable reaction term,

$$u_t = \gamma \Delta u + f(u, \alpha), \qquad 0 < \alpha < 1. \tag{15}$$

In this thesis we choose the constant $\gamma = 0.05$ and the bistable reaction term $f(u, \alpha)$ is defined by

$$f(u) = u(1 - u)(u - \alpha) \tag{16}$$

which is plotted in Figure 1. This function has the same characteristics as case 3, namely two states $\{0, 1\}$ that are stable under the dynamics $\dot{u} = f(u)$ and one unstable state $\{\alpha\}$ in between.

Figure 1: $f(u, 0.25) = u(1 - u)(u - 0.25)$.

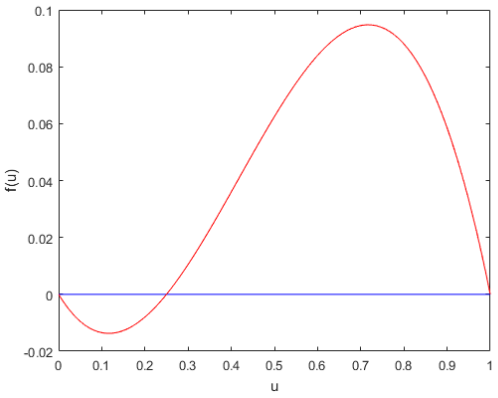

Lately it has become clear that some situations cannot be described in continuous space, for example the nervous system, see Figure 2.

Consider a signal that travels along an axon. The signal travels quickly at the parts where the axon is covered with myelin sheath. At the small parts which are not covered with myelin sheath the signal travels very slow. When we demand to simulate how the signal moves through the nerves, we need to measure with two different time scales. This makes it difficult to get correct information about the behaviour of the signals. Since the signals travels quickly through the parts which are covered with myelin sheath, we can simulate the signals travelling through the axon like it jumps from the end of a part of the axon without myelin sheath, to the beginning of the next part on the axon without myelin sheath. This provides us a discrete situation.

Figure 2: Part of the nervous system [1].

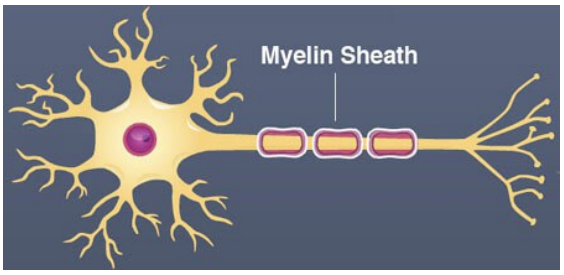

When a situation is not continuous in time or space, but is still modelled by a reaction-diffusion equation which assumes that the situation is continuous in time and space, we get incorrect information about the behaviour of the solution. This thesis will therefore also focus on the behaviour of the Lattice Differential Equation based on the PDE given in (15). The Lattice Differential Equation is

$$\dot{u}_{i,j} = \gamma(\Delta^+ u)_{i,j} + f(u_{i,j}, \alpha) \tag{17}$$

in which $f(u_{i,j}, \alpha)$ is the same bistable reaction term as by the PDE.

The special solution we focus on is an expansion wave, this is the solution which arises when there is a large enough perturbation. In other words, when we have LDE with initial conditions that can be interpreted as everywhere the conditions are zero except for a compact region where the conditions are one, then the solution of the PDE is called an expansion wave. The shape of this expansion wave is closely related to the behaviour of another special class of solutions to (17), namely planar travelling waves.

2 Behaviour of the Partial Differential Equation

We directly see that $u = 0$, $u = \alpha$ and $u = 1$ are solutions of (15), that do not vary in time and space. In this section we are interested in solutions for which $u(x, y, t) \in [0, 1]$ for all $x, y \in \mathbb{R}^2$ and $t \geq 0$. We start in section 2.1 by looking at special solutions called travelling waves. In section 2.2 we use them to make general solutions concerning the behaviour of (15).

2.1 Travelling wave solution

We look for a special class of solutions that maintain their shape as they travel through space. These kind of solutions are called travelling waves and can be written in the form $u(x, t) = \phi(x + ct)$. Here we call ϕ the wave profile, $\xi(x, t) = x + ct$ the travelling wave coordinate and c the wavespeed. This gives us the travelling wave solution

$$u(x, t) = \phi(\xi(x, t)). \tag{18}$$

In section 2.2 we will see that these waves can be very useful when trying to understand the behaviour of general solutions of the PDE. Substituting the travelling wave in (15) gives us the ordinary differential equation

$$c\phi'(\xi) = \gamma\phi''(\xi) + f(\phi(\xi), \alpha), \tag{19}$$

which can be solved easily. Nevertheless we first look at the two-dimensional PDE.

In two dimensions, we have the travelling wave Ansatz $u(x,y,t) = \phi(k_1x + k_2y + ct)$, with $\xi(x,y,t) = k_1x + k_2y + ct$. Here (k_1, k_2) is the direction of the wave and therefore we set $k_1^2 + k_2^2 = 1$, which can be chosen as $k_1 = \cos(\theta)$ and $k_2 = \sin(\theta)$. The wavespeed c is not direction dependent and substituting $\phi(\xi(x,y,t))$ in (15) gives us

$$c\phi'(\xi) = \gamma(k_1^2\phi''(\xi) + k_2^2\phi''(\xi)) + f(\phi(\xi), \alpha).$$

Since $k_1^2 + k_1^2 = 1$, we can write above equation as an ordinary differential equation, which is the same as the ordinary differential equation for one dimension

$$c\phi'(\xi) \quad = \gamma\phi''(\xi) + f(\phi(\xi), \alpha). \tag{20}$$

Notice that the direction disappeared out of the equation. This gives us the same wave profile ϕ and speed c for every direction.

We try to verify if the wave profile $\phi(\xi) = \frac{1}{2} + \frac{1}{2}\tanh(\beta\xi)$ leads to a travelling wave solution. Therefore we need the derivative with respect to ξ, the second derivative with respect to ξ and we need $f(\phi(\xi), \alpha)$

$$\begin{array}{ll} f(\phi(\xi),\alpha) & = \frac{1}{8} - \frac{\alpha}{4} + \frac{1}{8}\tanh(\beta\xi) - \frac{1}{8}\tanh^2(\beta\xi) + \frac{1}{4}\tanh^2(\beta\xi)\alpha - \frac{1}{8}\tanh^3(\beta\xi) \\ \phi'(\xi) & = \frac{1}{2}\beta - \frac{1}{2}\beta\tanh^2(\beta\xi) \\ \phi''(\xi) & = -\tanh(\beta\xi)\beta^2 + \tanh^3(\beta\xi)\beta^2. \end{array} \tag{21}$$

Substitution of the equations of (21) in ODE (20) gives us

$$\frac{c\beta}{2} - \frac{c\beta}{2}\tanh^2(\beta\xi) = \frac{1}{8} - \frac{\alpha}{4} + (\frac{1}{8} - \gamma\beta^2)\tanh(\beta\xi) + (\frac{\alpha}{4} - \frac{1}{8})\tanh^2(\beta\xi) + (\gamma\beta^2 - \frac{1}{8})\tanh^3(\beta\xi). \tag{22}$$

To satisfy equation (21) we need to solve β and c from the equations

$$\frac{c\beta}{2} + \frac{\alpha}{4} - \frac{1}{8} = 0, \qquad \gamma\beta^2 - \frac{1}{8} = 0, \qquad -\frac{c\beta}{2} - \frac{\alpha}{4 + \frac{1}{8}} = 0 \qquad \text{and} \qquad -\gamma\beta^2 + \frac{1}{8} = 0. \tag{23}$$

Solving gives $\beta = \sqrt{\frac{1}{8\gamma}}$ and

$$c(\alpha) = (\frac{1}{4} - \frac{\alpha}{2})\sqrt{(8\gamma)}.$$

For $\gamma = 0.05$, we get $\beta = \frac{\sqrt{10}}{2}$ and

$$c(\alpha) = \frac{1}{\sqrt{10}}(\frac{1}{2} - \alpha). \tag{24}$$

As shown in Figure (3), our travelling wave solution has the form

$$\phi(\xi) = \frac{1}{2} + \frac{1}{2}\tanh\left(\frac{\sqrt{10}}{2}\xi\right). \tag{25}$$

The travelling wave solution has two limits, namely

$$\lim_{\xi \to -\infty} \phi(\xi) = 0 \qquad \text{and} \qquad \lim_{\xi \to \infty} \phi(\xi) = 1. \tag{26}$$

Figure 3: The wave $\phi(\xi)$.

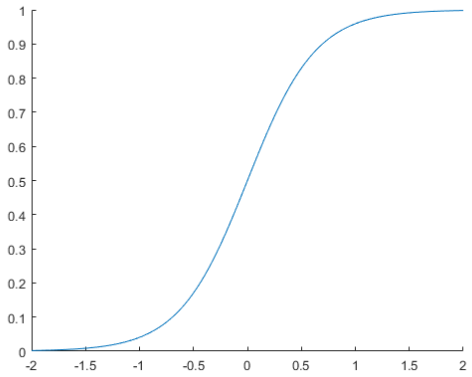

In Figure 4(a) we see that for $\alpha < 0.50$ the speed of the travelling wave is positive, causing the wave moving in the direction where the solution is 0, see Figure 4(b).

Figure 4: The speed and direction of the travelling wave.

(a) The speed c versus α for the PDE.

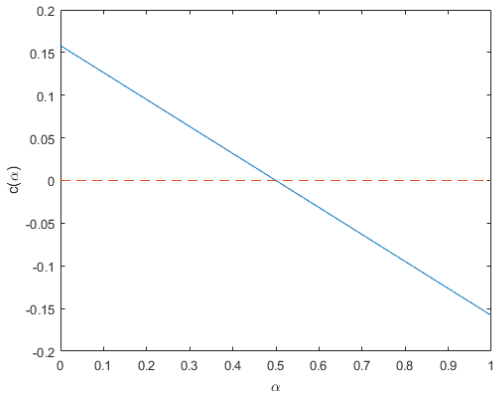

(b) Travelling direction of the wave.

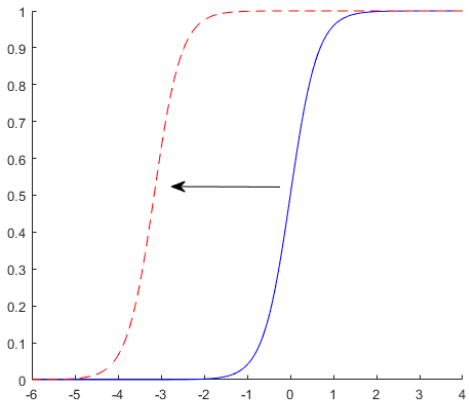

2.2 Comparison principle

To get a better idea of the behaviour of the general solution we use the comparison principle. The comparison principle says that if we can find, *a subsolution*, and *a supersolution*, then the solution to the PDE can be captured between the sub- and supersolution for all t.

We first introduce the notion of a subsolution:
Definition 1. We say that $u^-(x,y,t)$ is a *subsolution* if

$$u_t^-(x,y,t) \leq \Delta u^-(x,y,t) + f(u^-(x,y,t),\alpha) \tag{27}$$

holds for all $t \geq 0$ and for all $(x,y) \in \mathbb{R}^2$.

We further introduce the notion of a supersolution:
Definition 2. We say that $u^+(x,y,t)$ is a *supersolution* if

$$u_t^+(x,y,t) \geq \Delta u^+(x,y,t) + f(u^+(x,y,t),\alpha) \tag{28}$$

holds for all $t \geq 0$ and for all $(x,y) \in \mathbb{R}^2$.

With these definitions we can formulate the comparison principle [4].

Theorem 1. Suppose that $u^-(x,y,t)$ is a subsolution and $u^+(x,y,t)$ is a supersolution. Furthermore suppose that $u^-(x,y,0) \leq u^+(x,y,0)$ holds. Then for all $(x,y) \in \mathbb{R}^2$ we have

$$u^-(x,y,t) \leq u^+(x,y,t) \qquad \text{for } t \geq 0.$$

The above definitions and theorem also holds for a subsolution $u^-(x,t)$ and supersolution $u^+(x,t)$ in one dimension.

Examples of sub- and supersolutions are $u^+ \equiv 1$ and $u^- \equiv 0$. Also $u^+ \equiv 0$ and $u^- \equiv 1$ are respectively super- and subsolutions. Notice that for these examples hold that they are also solutions of the PDE. Not all sub- and supersolutions are also solutions, however, all solutions of the PDE are sub- and supersolutions. We construct a specific subsolution, such that we can say something about the behaviour of a solution, however, this subsolution is not an exact subsolution.

For a specific α, the waves in all directions have the same shape and speed. So if we want to construct a subsolution, we only have to construct a subsolution for one direction. We look at the horizontal wave, where $\theta = 0$ and $(k_1, k_2) = (1, 0)$.

We know that there exists a $u(x,t) = \phi(\xi)$ which satisfies equation (20) upon with $\xi = x + ct$, and which is also a subsolution since every solution is a subsolution.

The specific subsolution we want to construct is a subsolution which has the same shape as the travelling wave solution ϕ, it only lies lower than the solution and travels slightly slower.

Lemma 1. There exists a $K > 0, \epsilon_0 > 0, \beta_0 > 0$, such that for all $0 < \epsilon \leq \epsilon_0$ and $0 \leq \beta \leq \beta_0$, the function

$$u^-(x,t) = \phi(x + ct - Z(t)) - z(t)$$

with $z(t) = \epsilon e^{-\beta t}$, $Z'(t) = Kz(t)$ and $Z(0) = 0$ is a subsolution of $u(x,t)$.

Proof. Since we want to check if $u^-(x,t)$ is a subsolution of $u(x,t)$ we need to check if

$$J = u_t^- - \gamma \Delta u^- - f(u^-) \leq 0 \tag{29}$$

holds. We therefore compute

$$\begin{array}{ll} u_t^- & = (c - Kz(t))\phi'(x + ct - Z(t)) - z'(t) \\ \Delta u^- & = \phi''(x + ct - Z(t)) \\ f(u^-) & = f\left(\phi(x + ct - Z(t)) - z(t)\right). \end{array} \tag{30}$$

Substitution of (30) in J gives us the expression

$$\begin{aligned} J = \quad & (c - Kz(t))\phi'(x + ct - Z(t)) - z'(t) - c\phi'(x + ct - Z(t)) + f(\phi(x + ct - Z(t)) \\ & -f(\phi(x + ct - Z(t)) - z(t)). \end{aligned}$$

From this expression the first part and the third part eliminate each other. This gives us a smaller expression for J, namely

$$J = \quad -Kz(t)\phi'(x + ct - Z(t)) - z'(t) + f(\phi(x + ct - Z(t)) - f(\phi(x + ct - Z(t)) - z(t)). \tag{31}$$

We know that our solution $\phi(\xi)$ is a non decreasing function, thus $\phi'(\xi) \geq 0$. Furthermore $z(t) > 0$ and $z'(t) = -\beta z(t) < 0$ holds. We need more information to state that $J \leq 0$.

We take a closer look at $f(\phi(x + ct - Z(t)) - f(\phi(x + ct - Z(t)) - z(t))$. For all continuous functions we can say that the growth of the function over a distance v, is smaller or equal to the the largest absolute value of steepness in the interval $(u, u + v)$ multiplied by the distance v. This gives us the upper limit

$$|f(u + v) - f(u)| \leq \left(\sup_{0 \leq t \leq 1} |f'(u + tv)| \right) \mid v \mid$$

in which we set the supremum as $\sup_{-1 \leq u \leq 2} |f'(u)| = M$. In our case the distance v is $z(t)$, therefore

$$f(\phi(x + ct - Z(t))) - f(\phi(x + ct - Z(t)) - z(t)) \leq Mz(t).$$

The expression for J becomes

$$J \leq -Kz(t)\phi'(x + ct - Z(t)) - z'(t) + Mz(t).$$

To ensure that $J \leq 0$, we need to choose ϵ_0 and β_0 carefully. Suppose that $\phi'(x+ct-Z(t)) \geq \kappa_0$, with $\phi'(\kappa_-) = \phi'(\kappa_+) = \kappa_0$ and $\kappa_- < \kappa_+$, see Figure 5(a). Then we have the inequality

$$-Kz(t)\phi'(x + ct - Z(t)) \leq -K\kappa_0 z(t).$$

In particular we need to ensure

$$-K\kappa_0 z(t) + \beta z(t) + Mz(t) \leq 0,$$

which is satisfied provided $-K\kappa_0 \geq \beta + M$. By choosing $K\kappa_0 \geq 2M$ and $\beta_0 \leq M$, we satisfy that inequality. As a result we can conclude that

$$J \leq -2Mz(t) + Mz(t) + Mz(t) = 0,$$

for $K\kappa_0 \geq 2M$ and $\beta_0 \leq M$.

To ensure that $u^-(x,t)$ is a subsolution, we also need to check if $J \leq 0$ for $\phi'(x+ct-Z(t)) \leq \kappa_0$, with $\phi'(\kappa_-) = \phi'(\kappa_+) = \kappa$ and $\kappa_- < \kappa_+$. Therefore we need to set $\phi(\kappa_-) = u_-$ and $\phi(\kappa_+) = u_+$, see Figure 5(b). We choose κ_0 small, such that $f'(u_-) < -\eta$ and $f'(u_+ - \epsilon_0) < -\eta$, with $\eta = \frac{1}{2}\min(-f'(0), -f'(1))$.

For $\phi'(x + ct - Z(t)) \leq \kappa_0$ follows that $\phi(x + ct - Z(t)) \leq u_-$ or $\phi(x + ct - Z(t)) \geq u_+$. For $\phi(x + ct - Z(t)) \leq u_-$ holds that $\phi(x + ct - Z(t)) - z(t) \leq u_-$ too. Together with the knowledge that $\sup_{x \leq u_-} f'(x) = f'(u_-)$ it provides us with the upper limit

$$f(\phi(x + ct - Z(t)) - f(\phi(x + ct - Z(t)) - z(t)) < -\eta z(t). \tag{32}$$

Figure 5: The choice for κ_0.

(a) κ_0, κ_- and κ_+ in $\phi'(\xi)$.

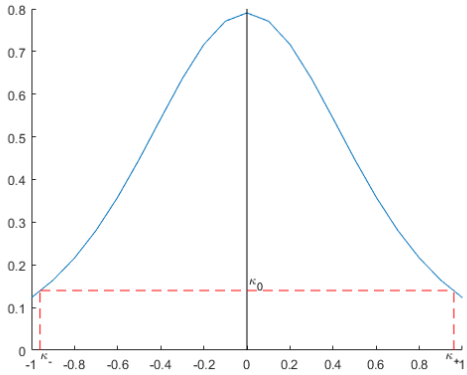

(b) κ_-, κ_+, u_- and u_+ in $\phi(\xi)$.

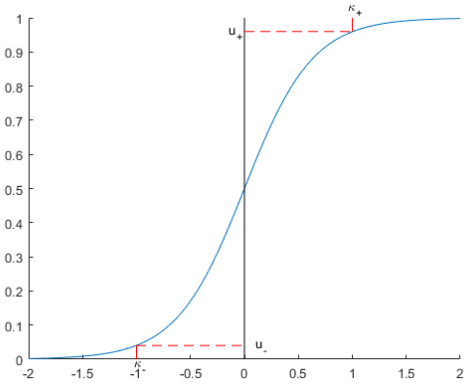

Notice that for $\phi'(x+ct+Z(t)) < \kappa_0$ the term $K\kappa_0\phi'(x+ct+Z(t))$ is positive, but very small. For J we get

$$J \leq \beta_0 z(t) - \eta z(t) \tag{33}$$

Since we need $J \leq 0$, we choose $\beta_0 < \eta$.

Finally we look at the situation where $\phi'(x+ct-Z(t)) \leq \kappa_0$, with $\phi(x+ct-Z(t)) \geq u_+$ and $\phi(x+ct-Z(t))-z(t) \geq u_+-\epsilon_0$. Together with the knowledge that $\sup_{x\geq u_+-\epsilon_0} f'(x) = f'(u_+-\epsilon_0)$, it gives us the upper limit (32), which in turn gives

$$J \leq \beta_0 z(t) - \eta z(t). \tag{34}$$

Since we need $J \leq 0$, we choose $\beta_0 < \eta$.

So for both $\phi(x+ct-Z(t)) \leq u_-$ and $\phi(x+ct-Z(t)) \geq u_+$, there exists a ϵ_0 and β_0 such that $J \leq 0$. Previously we saw that for $\phi'(x+ct-Z(t)) \geq \kappa_0$, there exists a ϵ_0 and β_0 such that $J \leq 0$. Thus there exists a subsolution of the form $u(x,t) = \phi(x+ct-Z(t)) - z(t)$. □

In the same way we can find a supersolution.

Lemma 2. There exists a $\epsilon_0 > 0, \beta_0 > 0$, such that for all $0 < \epsilon \leq \epsilon_0$ and $0 \leq \beta \leq \beta_0$, the function

$$u^+(x,t) = \phi(x+ct+Z(t)) + z(t)$$

with $z(t) = \epsilon e^{-\beta t}$, $Z(t) = Kz(t)$ and $Z(0) = 0$ is a supersolution of $u(x,t)$.

Proof. See *proof* of Lemma 1. □

We constructed a subsolution for our solution, which means that our solution always has to be above the subsolution. Analyzing Figure 6a shows us that when the subsolution moves to the left, the solution also has to move to the left, otherwise it would not be above the subsolution.

Lemma 3. Consider the PDE (15) and assume that $c(\alpha) > 0$. Let $u(x,0) = u_0(x)$ be the initial condition of (15) and let $u(x,t)$ be the solution. Assume that $u_0(x) \in [0,1]$ for all x and that

$u_0(x) \geq 1 - \delta$ for all $x > 0$, for some sufficiently small $\delta > 0$. Then for all $x_* \in \mathbb{R}$ we have the limit

$$\lim_{t\to\infty} u(x_*, t) = 1.$$

Proof. We use the subsolution $u^-(x-L,t)$ from Lemma 1. To ensure that $u^-(x-L,t)$ lies under $u_0(x)$ we set $\epsilon = 2\delta$. Since we have $u_0(x) \in [0,1]$, we need to choose L large enough to ensure that $u^-(0-L,t) = 0$. In Figure 4b we have seen the direction of the travelling wave solution of (15). Since our subsolution has the same characteristics we can conclude that it travels in the same direction. Thus the subsolution will push u_0 to $u_0(x,t) = 1 - \delta$ for all x, see Figure 6a. Since

$$\lim_{t\to\infty} z(t) = 0, \tag{35}$$

we can conclude that the subsolution $u^-(x-L,t)$ will push $u(x,t)$ to 1. □

Figure 6: Pushing subsolutions.

(a) Solution $u(t)$ is pushed to the left by the subsolution $u^-(t)$.

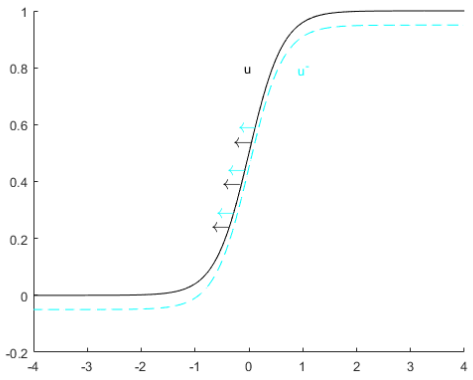

(b) Solution $u(t)$ is pushed outwards by the subsolution $u^-(t)$.

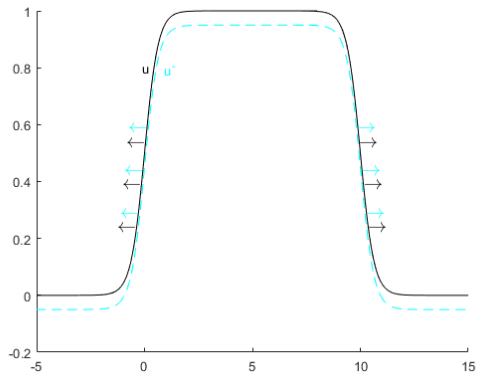

In the case that the perturbation is not high enough, there will not arise an expansion wave. This can also be proven with the comparison principle.

Lemma 4. Consider the PDE (15). Let $u(x,0) = u_0(x))$ be the initial condition of (15) and let $u(x,t)$ be the solution. Assume that there is $\epsilon > 0$ so that $u_0(x) \in [0, \alpha - \epsilon]$ for all x. Then for all $x_* \in \mathbb{R}$ we have

$$\lim_{t\to\infty} u(x_*, t) = 0.$$

Proof. We use the supersolution $u^+(x,t)$ for the solution of (15), with initial conditions $u^+(x,0) = \alpha - \epsilon$. For this supersolution we have $\frac{d}{dt}u^+(x,t) = f(u^+(x,t))$ for all $x \in \mathbb{R}$, thus it only depends on the reaction term of (15). The reaction term pushes solutions to zero when they are smaller than α. Thus the supersolution will be pushed down to zero, and hence

$$\lim_{t\to\infty} u^+(x,t) = 0 \tag{36}$$

for all $x \in \mathbb{R}$. Since the supersolution always has to be above the solution, the solution is pushed down to zero for all $x \in \mathbb{R}$. □

When we have a perturbation such that $u(x,t) > \alpha$ for $x \in [a,b]$ and for a sufficiently large L we have $a-b > L$ and $c(\alpha) > 0$, we get a similar result as in Lemma 3. First the interval $[a,b]$ will be pushed to 1 by the reaction term of (15), then we can build a subsolution by gluing $u^-(x,t)$ to its reflection $u^-(-x,t)$, which pushes the waves outwards, see Figure 6b. This procedure has been carried out in the classical paper by Aronson and Weinberger [3]. It is the general mechanism by which the expansion waves we consider in this thesis are pushed outwards.

Consider a perturbation in two dimensions, for which holds that $u(x,y,0) > 1-\delta$ for all $x \in [a,b]$ and $y \in [c,d]$. When $b-a$ and $d-c$ are big enough to let a wave arise, the same result as for one dimension holds. Namely each direction has its own solution, so for every direction we can build a subsolution, which pushes the solution to 1. So in two dimensions we have, under above assumptions

$$\lim_{t\to\infty} u(x,y,t) = 1. \tag{37}$$

As in the one-dimensional case, when the initial condition has $u(x,y,0) < \alpha-\epsilon$, there will not be an expansion wave. This can be proved by constructing a supersolution with $u^+(x,y,0) = \alpha - \epsilon$ for every direction, which pushes the solution to zero. This works in exactly the same way as Lemma 4.

3 Discretizing the Partial Differential Equation

To convert the PDE into an LDE we need the discrete laplacian in one dimension and in two dimensions. We start with the definition for one dimension.

Definition 3. The discrete laplacian in $\mathbb{R}$ is defined by

$$\Delta^+ u_i = u_{i+1} + u_{i-1} - 2u_i \tag{38}$$

with $i \in \mathbb{Z}$.

This can be motivated by using the definition of the derivative of a function $f(x)$. The derivative is defined by

$$f'(x) = \lim_{h\downarrow 0} \frac{f(x+h)-f(x)}{h} \qquad \text{and} \quad f'(x) = \lim_{h\uparrow 0} \frac{f(x-h)-f(x)}{-h}.$$

We can say that $2f'(x) = \lim_{h\to 0} \frac{f(x+h)-f(x-h)}{h}$ and thus $f'(x) = \lim_{h\to 0} \frac{f(x+h)-f(x-h)}{2h}$. This means for the second derivative that it can be defined by

$$f''(x) = \lim_{k\to 0} \frac{f'(x+k)-f'(x-k)}{2k} = \lim_{k\to 0}\lim_{h\to 0} \frac{\frac{f(x+k+h)-f(x+k-h)}{2h} - \frac{f(x-k+h)-f(x-k-h)}{2h}}{2k}.$$

Let $k = h$ then $f''(x) = \lim_{h\to 0} \frac{f(x+2h)+f(x-2h)-2f(x)}{(2h)^2}$. Since we can choose the length of h we can take $2h = h$, this gives

$$f''(x) = \lim_{h\to 0} \frac{f(x+h)+f(x-h)-2f(x)}{h^2}.$$

When we take $h = 1$ and substitute $u_i = f(i)$ we recover the discrete laplacian Δu_i.

In two dimensions we use the following definition.

Definition 4. The discrete laplacian in $\mathbb{R}^2$ is defined by

$$\Delta^+ u_{i,j} = u_{i+1,j} + u_{i-1,j} + u_{i,j-1} + u_{i,j+1} - 4u_{i,j} \tag{39}$$

with $i, j \in \mathbb{Z}$.

We will show this by using the definition of the partial derivatives of a function $f(x, y)$. In a two-dimensional space we have two directions, so we have 2 partial derivatives. The partial second derivative with respect to x is

$$\frac{\partial^2 f}{\partial x^2} = \lim_{h \to 0} \frac{f(x+h, y) + f(x-h, y) - 2f(x, y)}{h^2}.$$

The partial second derivative with respect to y is

$$\frac{\partial^2 f}{\partial y^2} = \lim_{h \to 0} \frac{f(x, y+h) + f(x, y-h) - 2f(x, y)}{h^2}.$$

When we add the above partial second derivatives we get

$$\Delta f(x, y) = \lim_{h \downarrow 0} \frac{f(x+h, y) + f(x-h, y) + f(x, y+h) + f(x, y-h) - 4f(x, y)}{h^2}$$

When we take $h = 1$ and substitute $u_{i,j} = f(i, j)$ we recover the discrete laplacian $\Delta u_{i,j}$.

4 Travelling wave of the Lattice Differential Equation

The LDE in one dimension is given by

$$\dot{u}_i = (\Delta^+ u)_i + f(u_i, \alpha), \tag{40}$$

in which the discrete laplacian is defined in (38). For the PDE we used the travelling wave Ansatz $u(x, t) = \phi(x + ct)$ to construct a travelling wave solution. For the LDE we also use a travelling wave Ansatz namely, $u_i(t) = \phi(i + ct)$, in which $\xi = i + ct$ is the travelling wave coordinate with wavespeed c.

Substitution of the travelling wave Ansatz $u_i(t) = \phi(i + ct)$ into (40) yields

$$c\phi'(i + ct) \quad = \phi(i - 1 + ct) + \phi(i + 1 + ct) - 2\phi(i + ct) + f(\phi(i + ct), \alpha).$$

Substitution of the travelling wave coordinate $\xi = i + ct$ gives

$$c\phi'(\xi) \quad = \phi(\xi - 1) + \phi(\xi + 1) - 2\phi(\xi) + f(\phi(\xi), \alpha) \tag{41}$$

The two-dimensional LDE is given by

$$\dot{u}_{i,j} = (\Delta^+ u)_{i,j} + f(u_{i,j}, \alpha), \tag{42}$$

in which the discrete laplacian is given by (39). For this two-dimensional LDE we use the travelling wave Ansatz $u_{i,j}(t) = \phi(k_1 i + k_2 j + ct)$, in which $\xi(t) = k_1 i + k_2 j + ct$ is the travelling wave coordinate with wavespeed c and direction coordinates $(k_1, k_2) = (\cos(\theta), \sin(\theta))$.

Substitution of the travelling wave Ansatz in the two-dimensional LDE gives,

$$\begin{aligned} c\phi'(k_1 i + k_2 j + ct) = \quad & \phi(k_1(i-1) + k_2 j + ct) + \phi(k_1(i+1) + k_2 j + ct) + \phi(k_1 i + k_2(j-1) + ct) \\ & + \phi(k_1 i + k_2(j+1) + ct) - 4\phi(k_1 i + k_2 j + ct) + f(\phi(_1 i + k_2 j + ct), \alpha) \end{aligned} \tag{43}$$

Substitution of the travelling wave coordinate $\xi(t)$ gives

$$c\phi'(\xi) = \phi\left(\xi - \cos(\theta)\right) + \phi\left(\xi + \cos(\theta)\right) + \phi\left(\xi - \sin(\theta)\right) + \phi\left(\xi + \sin(\theta)\right) - 4\phi(\xi) + f(\phi(\xi), \alpha) \tag{44}$$

Notice that the equation is direction dependent, thus the solution is also direction dependent. This means that for every direction we have a different solution. And thus for every direction we have a different relation between c and α, we notate the speed in direction θ by $c_\alpha(\theta)$. With a program coded by H.J.Hupkes in Fortran we determined for different values of α the speed $c_\alpha(\theta)$, for all θ.

We determined these wavespeeds by solving the boundary value problem

$$-\delta\phi''(\xi) + c\phi'(\xi) = \phi(\xi - \cos(\theta)) + \phi(\xi + \cos(\theta)) + \phi(\xi - \sin(\theta)) + \phi(\xi + \sin(\theta)) - 4\phi(\xi) + f(\phi(\xi), \alpha) \tag{45}$$

with the boundary conditions $\phi(x) = 0$ for $x \leq -L$ and $\phi(x) = 1$ for $x \geq L$, with additional requirements $\phi(0) = \alpha$ and $c' = 0$. Here we added the term $-\delta\phi''(\xi)$, with $\delta = 10^{-5}$ for a smoothening effect.

To get the polar plots of Figure 7 we plotted

$$c_\alpha(\theta)\cos(\theta), c_\alpha(\theta)\sin(\theta)). \tag{46}$$

In these polar plots we see that for different values of α, we get different shapes of the polar plots. The smaller α the more the shape looks like a circle, and for α close to $\alpha = 0.50$ the shape looks more like a flower and has more inlets. We also see that the closer α comes to $\alpha = 0.50$, the slower the largest speed becomes.

In Figure 8 we plotted $c_\alpha(0)$, here we see that, as for the PDE, the speed c is positive for $\alpha < 0.50$. Different than for the PDE we see that for $0.38 \leq \alpha \leq 0.50$ the value of c is almost zero. Roughly speaking, this means that horizontal and vertical movement is only possible for $\alpha < 0.38$.

Figure 7: $c_\alpha(\theta)$ polar plot for the LDE.

(a) $c_{0.10}(\theta)$ plot. (b) $c_{0.20}(\theta)$ polar plot. (c) $c_{0.25}(\theta)$ polar plot.

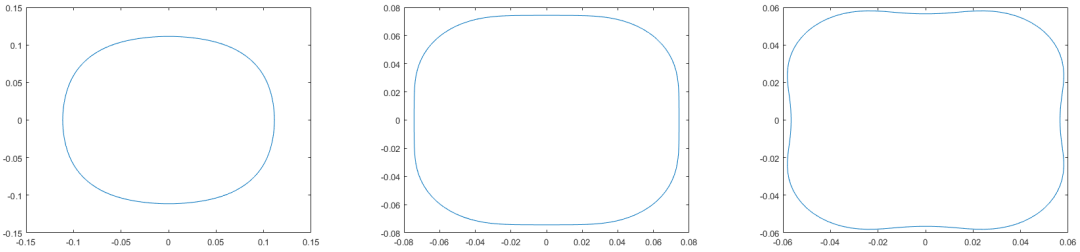

(d) $c_{0.30}(\theta)$polar plot. (e) $c_{0.37}(\theta)$ polar plot. (f) $c_{0.40}(\theta)$ polar plot.

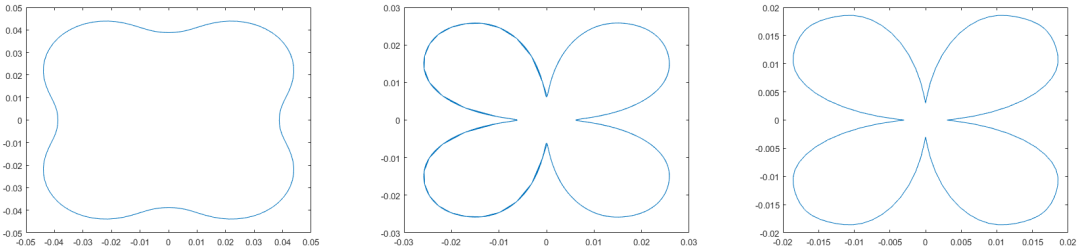

(g) $c_{0.45}(\theta)$ polar plot. (h) $c_{0.49}(\theta)$ polar plot.

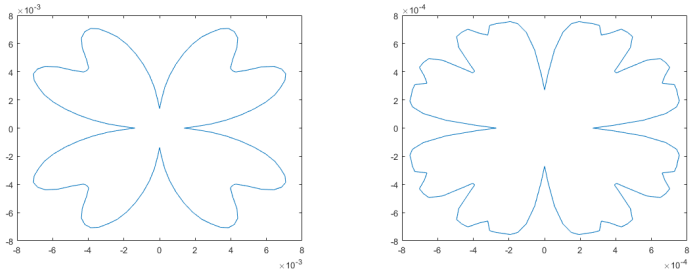

Figure 8: The speed c versus α for the LDE, at angle $\theta = 0$.

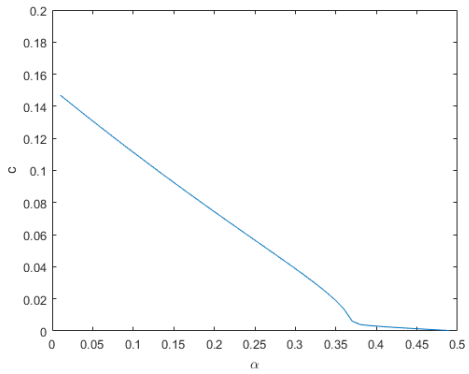

5 Behaviour of the Lattice Differential Equation

5.1 Comparison principle for the LDE

In discrete spatial domains the same comparison principle as in continuous domains applies. It says that if we can find *a subsolution* and *a supersolution*, then solutions between the sub- and supersolution can be captured. We first introduce the notion of a subsolution:
Definition 5. We say that $u^-_{i,j}(t)$ is a *subsolution* if

$$\dot{u}^-_{i,j}(t) \leq (\Delta^+ u)^-_{i,j}(t) + f(u^-_{i,j}(t), \alpha) \tag{47}$$

holds for all $t \geq 0$ and for all $(i,j) \in \mathbb{Z}^2$.

We also introduce the notion of a supersolution:
Definition 6. We say that $u^+_{i,j}$ is a *supersolution* if

$$\dot{u}^+_{i,j}(t) \geq (\Delta^+ u)^+_{i,j}(t) + f(u^+_{i,j}(t), \alpha) \tag{48}$$

holds for all $t \geq 0$ and for all $(i,j) \in \mathbb{Z}^2$.

With these definitions we can formulate the comparison principle [4].

Theorem 2. Suppose that $u^-(t)_{i,j}$ is a subsolution and $u^+_{i,j}(t)$ is a supersolution. And suppose that $u^-_{i,j}(0) \leq u^+_{i,j}(0)$ holds. Then for all $(i,j) \in \mathbb{Z}^2$

$$u^-_{i,j}(t) \leq u^+_{i,j}(t) \qquad \text{for } t \geq 0.$$

Above definitions and theorem also holds for a subsolution $u^-_i(t)$ and supersolution $u^+_i(t)$ in one dimension.

Examples of sub- and supersolutions for the LDE are $u^+ \equiv 1$ and $u^- \equiv 0$. Also $u^+ \equiv 0$ and $u^- \equiv 1$ are respectively super- and subsolutions. Notice that for these examples hold that they are, like for the PDE, solutions of the LDE. Not all sub- and supersolutions are also solutions, however all solutions of the LDE are sub- and supersolutions. For the PDE we constructed a specific subsolution, that says something interesting about the behaviour of general solutions. In exactly the same way such a subsolution for the LDE, can be constructed.

Lemma 9. There exists a $K > 0, \epsilon_0 > 0, \beta_0 > 0$, such that for all $0 < \epsilon \leq \epsilon_0$ and $0 \leq \beta \leq \beta_0$, the function

$$u^-_i(t) = \phi(i + ct - Z(t)) - z(t)$$

with $z(t) = \epsilon e^{-\beta t}$, $Z(t) = Kz(t)$ and $Z(0) = 0$ is a subsolution of $u_i(t)$.

Proof. The *proof* of Lemma 1 also works in the discrete setting. We only need to replace Δu by its discrete counterpart $\Delta^+ u_i$. Since this term drops out in the calculations of J, the same arguments can be used. □

Lemma 10. There exists a $K > 0, \epsilon_0 > 0, \beta_0 > 0$, such that for all $0 < \epsilon \leq \epsilon_0$ and $0 \leq \beta \leq \beta_0$, the function

$$u^+_i(t) = \phi(i + ct + Z(t)) + z(t)$$

with $z(t) = \epsilon e^{-\beta t}$, $Z(t) = Kz(t)$ and $Z(0) = 0$ is a supersolution of $u_i(t)$.

Proof. See the *proof* of Lemma 9. □

5.2 Numerical calculations to solve the LDE

To get an idea of the behaviour of general solutions we solved the LDE numerically with the ODE45 function in Matlab, see Appendix.

To solve the two-dimensional LDE, we made a $(n+1) \times (n+1)$-matrix u where the elements $u(i+1, j+1)$ for $i, j = 0, ..., n-1$ in the matrix corresponds to the values of the points in the lattice. The elements $u(1, j)$, $u(i, 1)$, $u(n+1, j)$ and $u(i, n+1)$ are the same as respectively $u(2, j)$, $u(i, 2)$, $u(n, j)$, $u(i, n)$. This is necessary to determine all the values of the $n \times n$-matrix du which corresponds to the time derivatives of the elements of u. Namely to determine the values, $du(i, j)$ have to be equal to $(\Delta^+ u)_{i,j} + f(u_{i,j}, \alpha)$, which is determined by the LDE (17). So to determine the values of $du(i, n)$ we need to calculate the laplacian, and therefore we need the values of $u(i-1, n)$, $u(i+1, n)$, $u(i, n-1)$ and $u(i, n+1)$. For the latter we need the $n+1$ column in the matrix u.

In order to obtain expansion waves, we saw in Lemma 7 that we need initial conditions where we have an area $A = (x, y) \in \mathbb{R}$, for which $\phi(x, t, 0) > \alpha$ when $x \in (a, b)$ and $y \in (c, d)$, with $b - a$ and $d - c$ sufficiently large. So to solve the LDE with ODE45 we made a $n \times n$-matrix Y0 which contains these initial conditions. The elements of Y0 are equal to zero except for a square with sides of length 20 in the middle. These have values $\text{Y0}(i, j) > \alpha$.

With the above statements we can numerically solve the LDE.

5.3 Numerical simulations

In this section we show the numerical simulations made by the matlab code explained in section 5.2.

The figures of the solutions we made are contour figures. These figures show us a two-dimensional figure of a three-dimensional solution. They show us the solution from above, so that we see the (x,y)-surface and it gives isolines of the height differences. This results in figures where we only see isolines at the place of the travelling wave. These isolines make closed shapes, for which in the inside of the isolines the solution is approximatly one and on the outside of the isolines the solution is aprroximatly zero.

In the Figures 10-14 we see the solutions for a specific α after different timesteps. Subfigure a shows the solution after 100 timesteps, subfigure b shows the solution after 400 timesteps and subfigure c shows the solution after 600 or 800 timesteps. Comparing the subfigures a we see that for different α we get little differences in the shape of the expansion waves. For the subfigures b we see accurate differences. Subfigures c shows us that the shape of the expansion waves is equal to the shapes of figure b. Those subfigures imply that for every α the expansion wave expands differently. We will discuss them together with the simulations.

Figure 9 shows the initial conditions for the LDE, these are the same for all α. The initial conditions are set on $(i, j, k) = (i, j, 0)$, except for a square in the middle, with sides of length 20 and angles of 90 degrees, this square has initial conditions $(i, j, k) = (i, j, 1)$.

Figure 9: Initial Condition of the simulations.

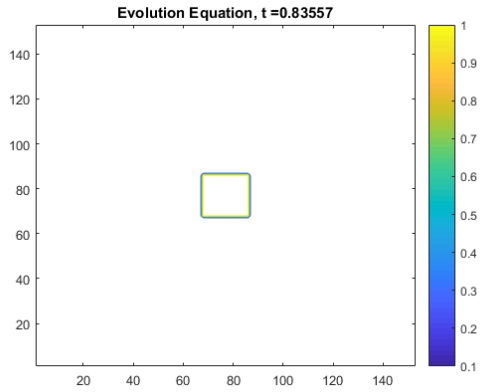

The simulation for $\alpha = 0.10$

In Figure 10 we see the expansion wave for $\alpha = 0.10$. In subfigure a the corners are rounder than at the initial conditions, but we still see some straight lines at the sides. In the simulation we saw that the expansion starts at the center of the sides, corresponding roughly to $\theta = 0, \frac{\pi}{2}, \pi, \frac{3\pi}{2}$ and then proceeds towards the corners, corresponding roughly to $\theta = \frac{\pi}{4}, \frac{4\pi}{4}, \frac{5\pi}{4}, \frac{7\pi}{4}$. Before the corners are reached, the expansion starts again at the center and the previous expansion still proceeds to the corners. The consequence of this behaviour is that the expansion in the corners are lagging behind on the expansion in de center of the sides. This results in a rounder expansion wave.

In subfigure b we see this result, the expansion wave does not have straight lines anymore. Although the expansion in the center of the sides expands faster than the corners, this does not result in a different shape after more than 400 timesteps, we see this result in subfigure c. Subfigure c shows us the shape of the expansion wave after 600 timesteps. The shape of this expansion wave is equal to the shape of the expansion wave in subfigure b. The only difference is that the surface is bigger.

Figure 10: The shape of the solution with $\alpha = 0.10$.

(a) After 100 timesteps. (b) After 400 timesteps. (c) After 600 timesteps.

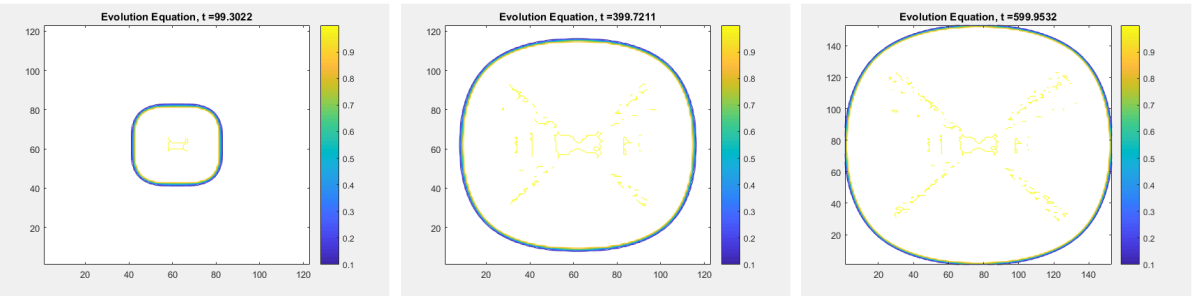

The simulation for $\alpha = 0.20$

In Figure 11 we see the expansion wave for $\alpha = 0.20$. In subfigure a the corners become a little bit rounder than the initial condition and we see some straight lines on the sides. Although the corners are round, they are less round than in subfigure 10a and the straight lines are longer. In the simulation we saw that, like for $\alpha = 0.10$, the expansion starts at the center of the sides. For $\alpha = 0.20$ we noticed that the expansion waits a little longer at the center of the sides before expanding again, than for $\alpha = 0.10$. This can be explained by Figure (8), which shows us that the expansion expands slower for larger α. In comparison with $\alpha = 0.10$, this is a more square expansion wave.

In Figure b we see that the straight lines have disappeared but the expansion wave is not as round as for $\alpha = 0.10$. For this solution also holds that the shape after 400 timesteps is the same shape after more than 400 timesteps, like subfigure c shows.

Figure 11: The shape of the solution for $\alpha = 0.20$.

(a) After 100 timestep.

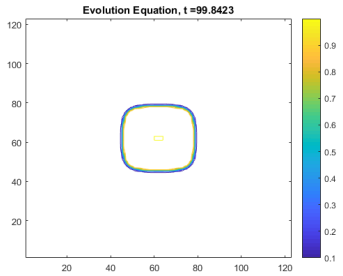

(b) After 400 timesteps.

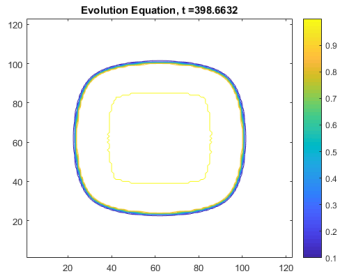

(c) After 600 timesteps.

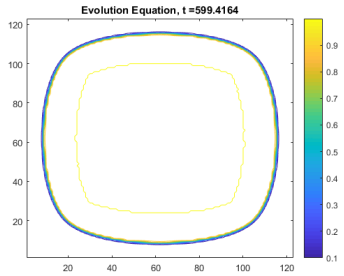

The simulation for $\alpha = 0.30$

In Figure 12 we see the expansion wave for $\alpha = 0.30$. In subfigure a the corners become a little bit rounder, but far less rounder than for $\alpha = 0.10$ and $\alpha = 0.20$, the straight lines are longer than for $\alpha = 0.10$ and $\alpha = 0.20$. In the simulation we saw that the expansion starts at the center of the sides too. The difference is that the expansion wave waits almost until the expansion reaches the corners, but it expands just before that moment at the center of the sides again. Finally we see an almost square expansion wave.

In Figure b we still see some straight lines but the expansion wave is rounder than subfigure a. For this solution also holds that the shape after 400 timesteps is the same shape after more than 400 timesteps, this is showed by subfigure c.

Figure 12: The shape of the solution for $\alpha = 0.30$.

(a) After 100 timestep. (b) After 400 timesteps. (c) After 800 timesteps.

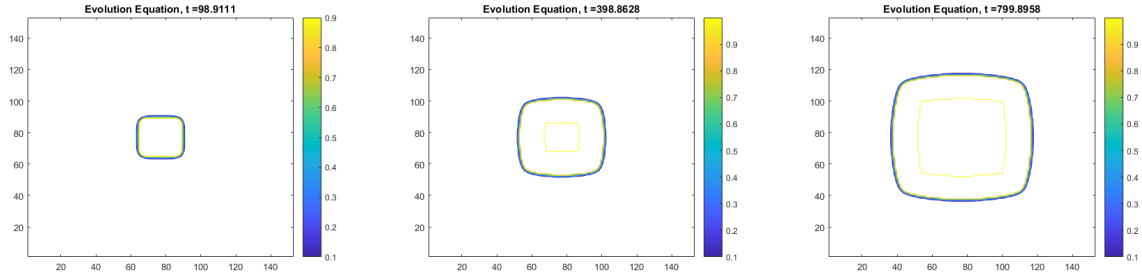

The simulation for $\alpha = 0.37$

In Figure 13 we see the expansion wave for $\alpha = 0.37$, this is a special expansion wave. In subfigure a we see the solution for t=100, at this point the expansion wave has not expand yet, the situation is the same as for the initial conditions, except for the fact that there arises a wave between the squared perturbation and the other part of the domain. The blue marks in the corner of the Figure are errors of matlab.

In subfigure b we see the same shaped expansion wave as in subfigure a, the only difference is that this one has a bigger surface, so the expansion wave has expand. For subfigure c holds the same as for subfigure b.

We see something different at subfigure d. The figure shows that when the expansion wave expands, the expansion starts at the center of the sides. The expansion has not reached the corners in this dubfigure. Eventually it will look like subfigure e.

Every time the expansion wave expands, the expansion starts at the center of the side and then proceeds to the corners. Only when the whole side has expand, then the expansion starts at the center of the sides agian. This means the shape of the expansion wave will always becomes a square again.

Figure 13: The shape of the solution for $\alpha = 0.37$.

(a) After 100 timesteps. (b) After 300 timesteps. (c) After 500 timesteps.

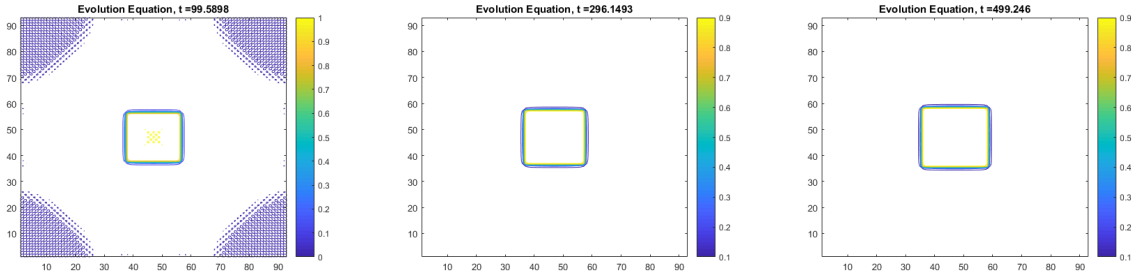

(d) After 580 timesteps. (e) After 700 timesteps.

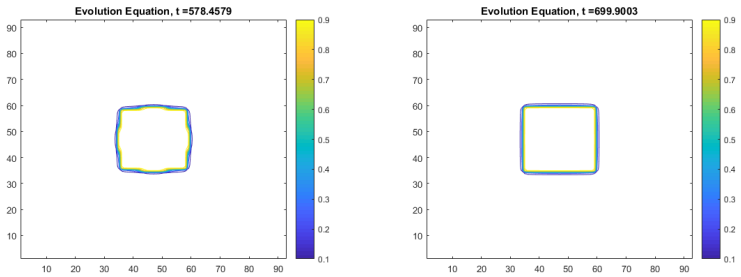

The simulation for $\alpha = 0.40$

In Figure 13 we see the expansion wave for $\alpha = 0.40$. In subfigure a, b and c, we see the same figure. This means that the expansion wave does not expand. For every $0.40 \leq \alpha \leq 0.49$ the expansion waves do not expand.

Figure 14: The shape of the solution for $\alpha = 0.40$.

(a) After 1 timesteps. (b) After 100 timesteps (c) After 400 timesteps.

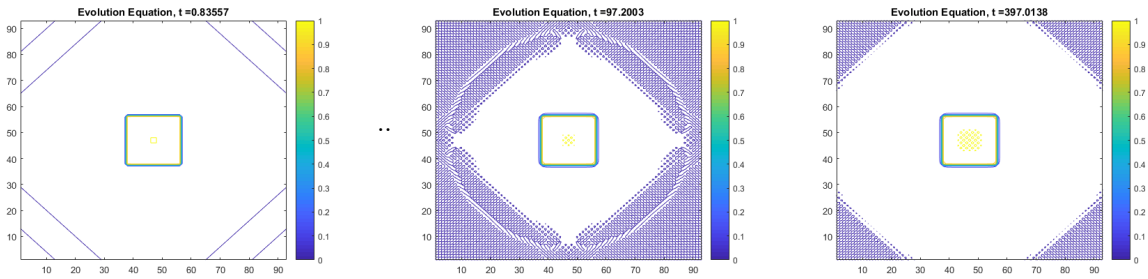

When we compare the simulations of the solutions, two differences stand out. The first one we already noticed in section 5, the smaller the value of α the faster the expansion wave expands. The second difference is that the smaller α is, the more round the perturbation becomes, therefore we make a conjecture in the next section.

6 The Wulff shape

The Wulff shape is mostly used to determine the equilibrium shape of a crystal. A crystal exists of surface free energy, if we plot that energy in a polar plot as a function of the orientation angle, we get a Wulff plot. When we create a shape that minimizes the surface energy of the crystal, than that shape is the Wulff shape of the crystal. This method is called the Wulff construction [5].

Conjecture: The final shape of the expansion wave can be found by applying the Wulff construction to the $c_\alpha(\theta)$ polar plot.

6.1 The Wulff construction

With the Wulff construction we determine the Wulff shape of the $c_\alpha(\theta)$ polar plots, and compare these with the shapes found in section 5.3. The method constructs the Wulff shape by the interior of perpendicular lines that are drawn on lines which connect the origin with a point on the $c_\alpha(\theta)$ polar plot, see Figure 15.

To determine the interior of the lines we use the equation $Ax \geq b$, where A is a $n \times 2$-matrix, the first column of A exists of the slopes of the perpendicular lines, and the second column are ones. b is a $n \times 1$-matrix where the elements of b are the y-coordinates where the perpendicular lines would cross the y-axis. The size of n is important for the accuracy of the Wulff shape, the bigger n the more accurate the Wulff shape is.

Figure 15: Creating a wulff shape with the wulff contruction.

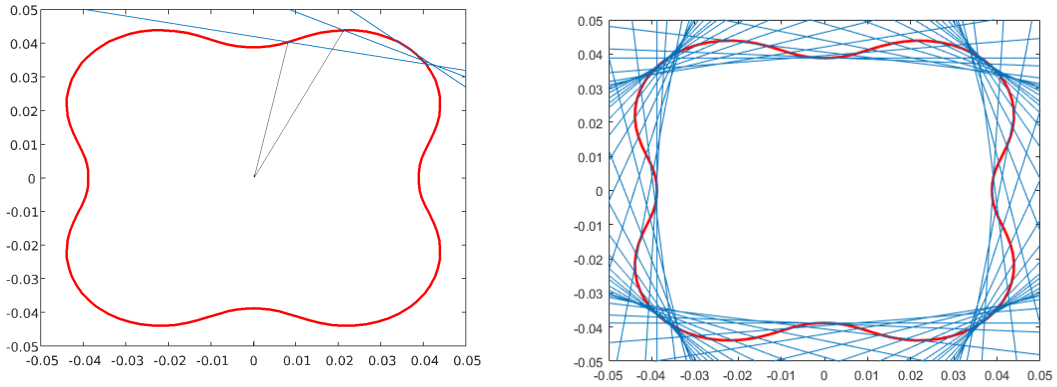

(a) Beginning of the construction, where the blue lines are the perpendicular lines.

(b) The Wulff shape is the interior of the blue perpendicular lines.

We use the notation of Figure (16) to determine the formula for the line L.

Figure 16: Constructing a Wulff shape.

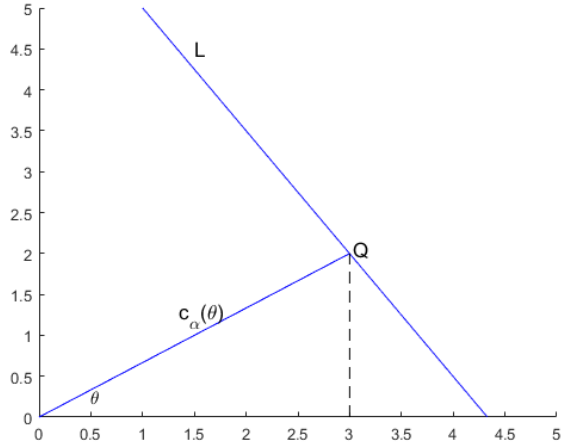

For the point Q we can say that it is placed at $Q = (c(\theta)\cos(\theta), c(\theta)\sin(\theta))$. The slope of the line $c_\alpha(\theta)$ is equal to

$$\frac{c(\theta)\sin(\theta)}{c(\theta)\cos(\theta)} = \tan(\theta). \tag{49}$$

This means that the slope of L is equal to

$$-\frac{1}{\tan(\theta)} = -\cot(\theta). \tag{50}$$

Thus the line L has the form $\cot(\theta)x + y = b$.

To determine the value of b, we substitute Q in the line L. This gives the equality $\cot(\theta)c(\theta)\cos(\theta) + c(\theta)\sin(\theta) = b$, so the value for b is

$$b = c(\theta)(\cot(\theta)\cos(\theta) + \sin(\theta)).$$

With the above calculations we can conclude that the line L has the form

$$\cot(\theta)x + y = c(\theta)(\cot(\theta)\cos(\theta) + \sin(\theta)).$$

Now we can determine the interior of the perpendicular lines by solving the inequalities.

$$\begin{pmatrix} -\cot(\theta_1) & 1 \\ -\cot(\theta_2) & 1 \\ \vdots & \vdots \\ -\cot(\theta_i) & 1 \\ \vdots & \vdots \\ -\cot(\theta_{n-1}) & 1 \\ -\cot(\theta_n) & 1 \end{pmatrix} \begin{pmatrix} x \\ y \end{pmatrix} \geq \begin{pmatrix} c(\theta_1)(\cot(\theta_1)\cos(\theta_1) + \sin(\theta_1)) \\ c(\theta_2)(\cot(\theta_2)\cos(\theta_2) + \sin(\theta_2)) \\ \vdots \\ c(\theta_i)(\cot(\theta_i)\cos(\theta_i) + \sin(\theta_i)) \\ \vdots \\ c(\theta_{n-1})(\cot(\theta_{n-1})\cos(\theta_{n-1}) + \sin(\theta_{n-1})) \\ c(\theta_n)(\cot(\theta_n)\cos(\theta_n) + \sin(\theta_n)) \end{pmatrix}$$

With matlab we solved these inequalities with the function *plotregion(A,b)*. This is an external utility for matlab and visualize solutions of the equation $Ax \geq b$. This gave us the Wulff shapes for different values of α, see Figure (17).

Figure 17: The Wulff shapes of the $c_\alpha(\theta)$ polar plots (colored in red) and the $c_\alpha(\theta)$ polar plots themselves.

(a) For $a = 0.10$. (b) For $a = 0.20$. (c) For $a = 0.30$.

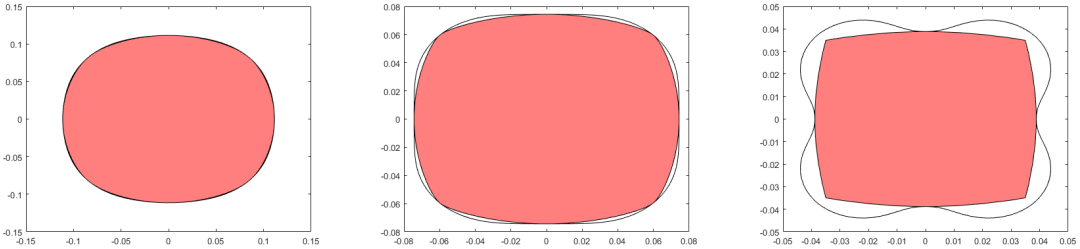

(d) For $a = 0.37$. (e) For $a = 0.40$. (f) For $a = 0.45$.

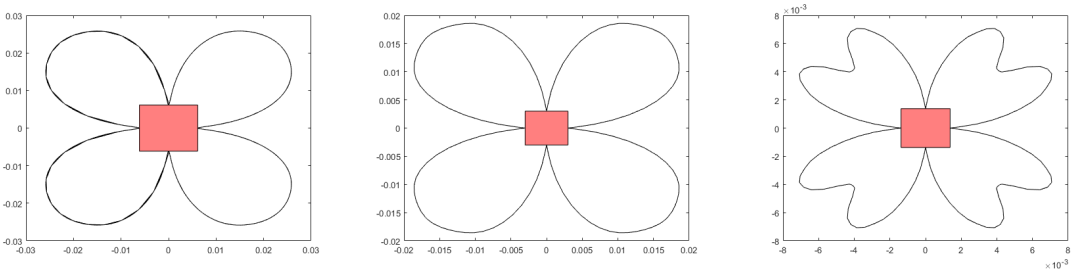

6.2 Comparison of the numeric simulations with the Wulff shapes

In the previous chapters we have seen how the expansion wave expands numerically and we have found the Wulff shape of the $c_\alpha(\theta)$ polar plots. The conjecture we made was that the Wulff shape would be the same shape as the final shape of the expansion wave. In this section we compare these numerical simulations with the Wulff shapes.

To compare these shapes we need the coordinates of the final shape of the numerical simulations and of the Wulff shapes. The coordinates of the Wulff shapes are saved in an array, which is used to made the Wulff shapes. On the other hand, the coordinates of the numerical simulations are not saved. The coordinates of the final shape were gained by finding for 350 angles the first points, seen from the origin, where the solution becomes smaller than 0.9. We achieved this by taking little steps in direction of the angle and checking for every step the value of the solution. When the value of the solution was smaller than 0.9 we saved the radius and the angle. With this information we determined the coordinates by calculating the equations

$$x = r\cos(\theta) \qquad \text{and} \qquad y = r\sin(\theta) \tag{51}$$

and with the radius we determined the angle with the biggest radius. The biggest radius is used to scale the final shape to a shape where the biggest radius is equal to 1.

Plotting these two shapes together gives the figures of Figure 18. In these figures we see a smooth shape, the Wulff shape and a rugged shape for the numerical simulation. The shape is rugged, since we had to determine the coordinates on a grid.

The figures show that the shapes are almost identical, except for some irregularities in the corners in the Figures 18(c) and (d). This can be explained by the fact that the numerical simulation is ran during a fixed amount of timesteps. As seen before in Figure 13d, it can occur that the middle waves already travelled, but the corners not yet. This makes it possible that the shapes of these forms eventually will end up in a Wulff shape, but differs in the transition to a bigger surface.

These comparisons gives us sufficient data to at least believe that the conjecture is credible.

Figure 18: Numeric simulations compared with the Wulff shapes.

(a) For $a = 0.10$.

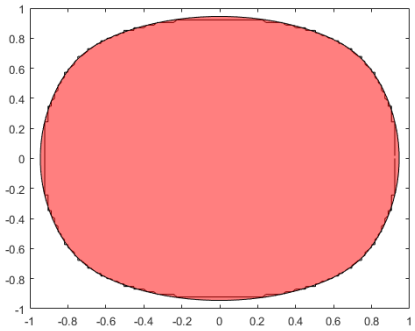

(b) For $a = 0.20$.

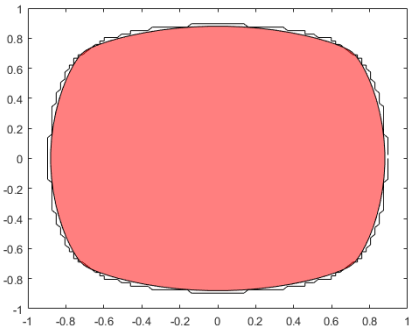

(c) For $a = 0.30$.

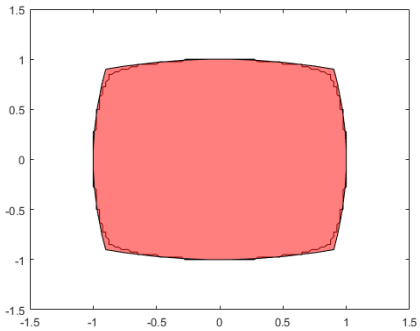

(d) For $a = 0.350$.

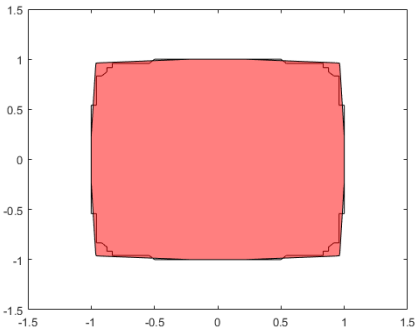

(e) For $a = 0.40$.

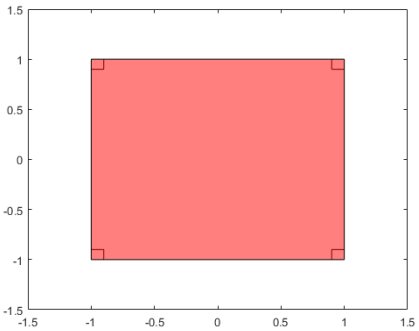

7 Discussion

In this thesis we focused on the behaviour of the expansion wave in a lattice.

We have seen that with sub- and supersolutions we can make general statements concerning the behaviour of solutions. Numerically we have analyzed the solution of a LDE, with as initial condition a perturbation that was big enough to become an expansion wave. We concluded that when we start with a squared perturbation, the expansion wave expands to a Wulff shape, made with the Wulff construction. However, we did not measure the time till infinity but to a finite time. We had to do this because the computer did not have enough memory. It would be interesting to see if it indeed converges to the Wulff shape found in this thesis, or that it maybe act differently than we found.

It would also be interesting to know if the expansion wave will always converge to the Wulff shape, independent of the form of the perturbation and what happens when we start with a circle or a star.

In this thesis we used a diffusion constant with value of 0.05 which had an influence on the results. However, if we would change this value, the question is whether this changes the fact that the expansion wave will converge to the Wulff shape.

Appendix A Matlab codes

A.1 Lattice differential equation 2D

```
function du1 = eqn2D(t,u1,n,a,ax,ap)

du1 = zeros(n*n,1);
du = reshape(du1,n,n);
u = reshape(u1(1:n*n),n,n);
ub = zeros(n+2,n+2);

for i=1:n
for j=1:n
    ub(i+1,j+1) = u(i,j);
end
end

for i=2:n+1
    ub(i,1)=ub(i,2);
    ub(i,n+2)=ub(i,n+1);
end

for j=2:n+1
    ub(1,j)=ub(2,j);
    ub(n+2,j)=ub(n+1,j);
end
ub(1,1)=ub(2,2);
ub(1,n+2)=ub(2,n+1);
ub(n+2,1)=ub(n+1,2);
ub(n+2,n+2)=ub(n+1,n+1);

for i=1:n
for j=1:n
    ubij=ub(i+1,j+1);
    f = ubij*(ubij-1)*(ubij-a);

    du(i,j) = ap*(-4*ubij+ub(i+2,j+1)+ub(i,j+1)+ub(i+1,j+2)+ub(i+1,j))-f;
end
end

du1(1:n*n) = reshape(du(1:n,1:n),n*n,1);


return
```

A.2 Code to solve the Lattice differential equation 2D, for $\alpha = 0.30$.

```
n=153; %uneven and mod 3 = 0
r=10;
```

```
a=0.30;
ax=0;
ap=0.05;

ce=(n-1)/2+1

%Set Initial Conditions
Y01=zeros(n*n,1);
Y0=reshape(Y01,n,n);
for i=1:n
for j=1:n
    val = max(abs(i-ce),abs(j-ce));
    if val < r
      Y0(i,j)=1;
   end
end
end

for j=1:n
   xall(j)=j;
end


Y01(1:n*n)=reshape(Y0(1:n,1:n),n*n,1);
TSPAN=[0 800];

options = odeset('RelTol',1e-6,'AbsTol',1e-8);
[TOUT,YOUT1] = ode45(@(t,y) eqn2D(t,y,n,a,ax,ap),TSPAN,Y01,options);
d=size(YOUT1);
tsteps = max(size(TOUT));
YOUT=reshape(YOUT1(:,1:n*n),d(1),n,n);
yfinal = squeeze(YOUT(tsteps,:,:));
xstart = ce;
ystart = ce;
theta = 0;
rvalues = zeros(2,350);
findRmax = zeros(1,350)

%Finding the Final Shape
for lijntje = 1:350
    theta = (2*pi*lijntje)/350
    rr = 1;
    while yfinal(round(xstart + rr * cos(theta)), ...
            round(ystart + rr*sin(theta))) > 0.9;
        rr = rr + 0.5;
    end
    findRmax(1,lijntje) = rr;
    rmax = max(findRmax);
    rvalues(1,lijntje)=round(rr*cos(theta));
```

```
    rvalues(2,lijntje)=round(rr*sin(theta));
end

for i=1:2
    j=1:350
    rvalues(i,j) = rvalues(i,j)/rmax;
end

%Saving the Final Shape
fileName = 'finalshape030t800.txt';
T = array2table(rvalues);
writetable(T, fileName);
T2 = readtable(fileName);
r2values = table2array(T2);

%Make Movie
f1 = figure;
hold off;
set(f1,'NextPlot','replacechildren');
winsize = get(f1,'Position');
winsize(1:2) = [0 0];
numframes = tsteps/10+1;
A = moviein(numframes, f1, winsize);
A(1) = getframe(f1,winsize);
first=zeros(r,r);
times=zeros(r,r);
ii=1;
for i = 1:tsteps
    ystep = squeeze(YOUT(i,:,:));
    for j=1:r
        for k=1:r
            if ystep(ce+j-1,ce+r+k-1) > 0.95 & first(j,k)==0
                first(j,k)=1;
                times(j,k)=TOUT(i);
            end
        end
    end
    if mod(i,10)==0
    figure(f1);
    [c,h] = contour(ystep); colorbar
    title(['Evolution Equation, t =', num2str(TOUT(i))])
    A(ii+1) = getframe(f1,winsize);
    ii=ii+1;
    end
end

%Play and Save Movie
movie(f1,A,1,30,winsize);
myVideo = VideoWriter('030t800.avi');
```

```
open(myVideo);
writeVideo(myVideo, A);
close(myVideo);
```

A.3 $c_\alpha(\theta)$ for $\alpha = 0.30$

```
close all

fileName = 'golfsnelheid005-030.txt';
T = readtable(fileName);
TasArray = table2array(T);

[m,n] = size(TasArray);

A1 = zeros(m,1);
A2 = zeros(m,1);
b = zeros(m,1);
P1 = zeros(1,m);
P2 = zeros(1,m);
for i=1:m
  A1(i,1) = -cos(TasArray(i,2));
  A2(i,1) = -sin(TasArray(i,2));
  b(i) = -abs(TasArray(i,3));
  P1(1,i) = abs(TasArray(i,3))*cos(TasArray(i,2));
  P2(1,i) = abs(TasArray(i,3))*sin(TasArray(i,2));
end


lb = [-3, -3];
ub = [3, 3];

plot(P1,P2);
```

A.4 Wulff shape of the $c_\alpha(\theta)$ for $\alpha = 0.30$

```
close all

fileName = 'golfsnelheid005-030.txt';
T = readtable(fileName);
TasArray = table2array(T);

[m,n] = size(TasArray);

A = zeros(m,2);
b = zeros(m,1);
P = zeros(2,m);

for i=1:m
  A(i,1) = -cos(TasArray(i,2));
```

```
  A(i,2) = -sin(TasArray(i,2));
  b(i) = -abs(TasArray(i,3));
  P(1,i) = abs(TasArray(i,3))*cos(TasArray(i,2));
  P(2,i) = abs(TasArray(i,3))*sin(TasArray(i,2));
end


lb = [-3, -3];
ub = [3, 3];

plotregion(A,b,lb,ub, 'w', 0.5, P);
```

A.5 Wulff shape of the $c_\alpha(\theta)$ compared with the numeric simulations for $\alpha = 0.30$

```
close all

fileName1 = 'golfsnelheid005-030.txt';
fileName2 = 'finalshape030t600.txt'
T1 = readtable(fileName1);
T2 = readtable(fileName2)
TasArray1 = table2array(T1);
TasArray2 = table2array(T2);

[m,n] = size(TasArray1);
[k,h] = size(TasArray2);

A = zeros(m,2);
b = zeros(m,1);
P = zeros(2,h);
wmin = min(abs(TasArray1(:,3)));

for i=1:m
    TasArray1(i,3)=TasArray1(i,3)/wmin;
end

for i=1:m
  A(i,1) = -cos(TasArray1(i,2));
  A(i,2) = -sin(TasArray1(i,2));
  b(i) = -abs(TasArray1(i,3));
end

dNormMin = 10;
for j=1:h
  dNorm =(TasArray2(1,j)^2 + TasArray2(2,j)^2)^0.5;
  if (dNorm<dNormMin)
      dNormMin=dNorm
  end
end
```

```
for  i=m+1:m+h
     j=i-m
   P(1,j) = TasArray2(1,j)/dNormMin;
   P(2,j) = TasArray2(2,j)/dNormMin;
end

P;

lb = [-3, -3];
ub = [3, 3];

figure; hold on;
xlim([-1.05 1.05]);
ylim([-1.05 1.05]);
plotregion(A,b,lb,ub, 'r', 0.5, P);
```

References

[1] Joseph Cohen. Top 55 ways to increase myelin naturally (and surprising facts). `https://selfhacked.com/blog/myelin/` (visited 27-07-2017).

[2] Aronson D.G. and Weinberger H.F. Nonlinear diffusion in population genetics, combustion, and nerve pulse propagation. .

[3] Aronson D.G. and Weinberger H.F. Multidimensional nonlinear diffusion arising in population genetics. *Advances in mathematics, Elsevier*, 30, .

[4] Berendsen J. Horizontal travelling waves on the lattice. Master's thesis, Leiden University.

[5] McCormack R.P. Roosen A.R. and Carter W.C. Wulffman: A tool for the calculation and display of crystal shapes. *Computational Materials Science, Elsevier*.